Rotational collectivity in shell-model wave functions for $A=20-28$ nuclei

M. Carchidi and B. H. Wildenthal
Department of Physics and Atmospheric Science, Drexel University, Philadelphia, Pennsylvania 19104
(Received 30 April 1987)

Results of shell-model calculations for $A=20-28$ nuclei are examined for manifestations of collective rotational structure. The calculations use the full set of $0d_{5/2}$-$1s_{1/2}$-$0d_{3/2}$ configurations and an empirical Hamiltonian which yields a comprehensive reproduction of $A=18-38$ spectroscopy. The shell-model eigenvalues and the electric quadrupole matrix elements calculated from the shell-model eigenfunctions are treated as pseudodata from which the parameters of the simple rotational model are extracted. These analyses reveal extended groups of model levels in several nuclei which can be characterized in terms of well-defined moments of inertia and stable intrinsic quadrupole deformations. The "bandlike" structure of these groups persists, with diminishing intensity, to the largest values of total angular momentum which can be generated within the *sd*-shell space for these nuclei. Other *sd*-shell nuclei which are sometimes considered as "rotational" exhibit some fragmentary evidence for rotational collectivity in the present analyses, but the characteristics of band structure are not sustained over extended sequences of levels.

I. INTRODUCTION

While rotational collectivity[1] conventionally is associated with heavy nuclei, for which a large number of shell-model orbitals presumably cooperate in generating the requisite deformations, evidence has also long been available for strong rotational collectivity in the light *sd*-shell region.[2-5] With the three active orbits of the *sd* shell ($0d_{5/2}$, $1s_{1/2}$, and $0d_{3/2}$), it is possible to make explicit shell-model calculations of the microscopic structure of levels which appear to have a rotational collective structural nature. Such calculations successfully reproduce many of the observed features of such levels which are responsible for their being characterized as "rotational." As in the case of heavy nuclei, the primary experimental evidence for rotational structure in the *sd* shell is the adherence of a sequence ("band") of levels to a $J(J+1)$ spacing of energies and electric quadrupole ($E2$) matrix elements (primarily transition matrix elements) which are consistent with their being generated from the angular-momentum coupling coefficients which relate states of particular J values in a "band" to the rotation of the deformed intrinsic state of the band and its permanent quadrupole moment. Qualitatively, the levels of a band are connected to each other by large $E2$ matrix elements, while $E2$ matrix elements between members of the band and other levels are weak to vanishing.

Given the vagaries of experimental feasibility, evidence for such a "rotational band" in a light nucleus typically consists of a sequence of level energies up through $J\approx 8$ and three to four quadrupole matrix elements. In fact, we will make only passing reference to actual experimental data in the present study. The essential features of almost all existing spectroscopic data on *sd*-shell nuclei are reproduced by current shell-model wave functions combined with appropriately renormalized effective operators.[6] Comparisons with experimental data[7] are included here principally as reassurance on this point and as illustrations of the relative paucity of the experimental evidence for postulating rotational structure in this region.

Our aim in this work is to establish in detail the degree to which realistic shell-model calculations in the complete $0d_{5/2}$-$1s_{1/2}$-$0d_{3/2}$ configuration space generate the characteristics of collective rotational motion. Our principal concerns are with energies and, moreso, the electric quadrupole matrix elements generated in the shell-model calculations. These calculated values of energy-level characteristics are free from the inescapable uncertainties and extensive (pervasive) lacunae of actual experimental results. They provide the basis for exhaustive and precise comparisons with the predictions of the simple rotational model. Thus, the degree to which these two descriptions are mutually consistent can be definitively established. Further, if one allows the assumption that the shell-model predictions are the best available estimates of unmeasurable experimental properties of *sd*-shell nuclei, then these comparisons can be extrapolated to estimate the degree to which actual *sd*-shell nuclei are governed by simple collective-rotational dynamics.

II. SHELL-MODEL ASPECTS

The *sd*-shell-model wave functions $|(sd)^n,\nu JTT_z\rangle$ we use in this study are calculated with the "universal *sd*" (USD) interaction[6] in the full *sd* shell-model space. The USD interaction was derived by making an iterative least-squares fit of shell-model eigenvalues to experimental level energies through the medium of the two-body matrix elements and single-particle energies of the effective model Hamiltonian. A critical factor in the success of this process was the assumption of a scaling factor of $(18/A)^{0.3}$ for the magnitudes of the two-body matrix elements used in the diagonalizations for levels of each given value of the mass number A. A total of 440 level energies were used in the data set which determined the USD interaction, these data being selected rather uni-

formly from over the entire $A=18-38$ mass range. These data were reproduced by the converged set of interaction parameters with an rms deviation of 140 keV. Another several hundred level energies in the region have subsequently been found to be predicted by the USD Hamiltonian with equal or better accuracy. A number of examinations of the wave functions obtained in the diagonalizations have been carried out[6] and have yielded the conclusion that this manifestation of the shell-model approach to *sd*-shell structure yields an accurate accounting of the experimentally observed single-nucleon, spin-observable, and shape-collective features of levels across the entire shell.

The model-space reduced matrix elements of the $E2$ operator, $A(E2)_{p/n}$ for protons and neutrons, respectively, are calculated in the conventional impulse approximation from the "USD" wave functions via the prescriptions given in Ref. 8. Input to these calculations require the one-body density matrix elements determined directly from the N-body "USD" shell-model wave functions *and* the single-particle matrix elements of the $O(E2)_{p/n}$ operator between the single-particle states of the model space. The radial integral parts of these single-particle matrix elements are calculated by using radial wave functions derived from the simple harmonic oscillator with a size parameter determined by the experimental rms charge radius of the ground state of the stable nucleus of each A value.

The total $E2$ proton transition matrix elements, $M(E2)_p$, which correspond to $E2$ values obtained with electromagnetic experimental probes, are obtained by renormalizing the model-space proton/neutron matrix elements $A(E2)_{p/n}$ to account for the effects of model-space truncations. The simplest procedure for renormalizing the shell-model matrix elements for electric quadrupole observables is to assign total "effective" charges $\bar{e}_p$ and $\bar{e}_n$ to the protons and neutrons which are active in the model space. Overall, the experimental values of the strengths of *sd*-shell $E2$ transitions are consistent with effective proton and neutron charges for the model particles which are constant, independent of state and mass.[8] Thus one can express the total model $E2$ matrix elements, $M(E2)_p$, as[8]

$$M(E2)_p=\bar{e}_p A(E2)_p+\bar{e}_n A(E2)_n \ . \tag{1}$$

In this study, the values[8] $\bar{e}_p$ and $\bar{e}_n$ are taken to be $1.35e$ and $0.35e$, respectively. The static electric quadrupole moment of a nuclear state Q, and the electric quadrupole transition strength $B(E2)$ are given in terms of $M(E2)_p$ by[9]

$$B(E2;i\rightarrow f)=M^2(E2)_p/(2J_i+1) \ , \tag{2}$$

and

$$Q=\sqrt{16\pi/5}\left[\frac{J(2J-1)}{(2J+1)(J+1)(2J+3)}\right]^{1/2} M(E2)_p\delta_{i,f} \ . \tag{3}$$

Values of Q and $M(E2)_p$ were thus calculated from the "USD" *sd*-shell model wave functions of Ref. 6. These values, along with the excitation energies obtained in the same model calculations, were then examined for the characteristics of simple rotational structure, as formulated in the next section.

The basic assumption of the nuclear shell model is that, to a first approximation, each proton and neutron moves independently in a potential that represents its average interaction with the other nucleons in the nucleus. In this sense, the shell model makes no initial assumptions about collective motion. The large $E2$ transition matrix elements characteristic of rotational collectivity can be partially realized in the shell-model framework via coherent interference between different components of strongly configuration-mixed states. In the present calculations, for example, the shell-model basis states, $\Phi_i(NJT)$, are represented as coupled products of the $(0d_{5/2})^{N_1J_1T_1}$, $(1s_{1/2})^{N_2J_2T_2}$, and $(0d_{3/2})^{N_3J_3T_3}$ configurations, where $N_1+N_2+N_3=A-16$ and the N_i,J_i,T_i give the number of nucleons in the orbit ρ_i and the value of the internal coupled angular momentum and isospin for that orbit. The eigenfunctions of the model space, $\Psi(NJT)$, are obtained as linear combinations of these basis states $\Phi_i(NJT)$, i.e.,

$$\Psi(NJT)=\sum_i a_i\Phi_i(NJT) \ ,$$

where the sum runs over all allowed basis states. The matrix element $A(E2)_{p/n}$ can be expressed as a linear combination of the basis-state matrix elements

$$A(E2)_{p/n}=\sum_i\sum_j a_i a_j'^{*}\langle\Phi_j(NJT)\|O(E2)_{p/n}\|\Phi_i'(NJ'T')\rangle \ . \tag{4}$$

"Collective" amplification in the shell-model calculation (i.e., large values of $|A(E2)|$) thus can result from having a large fraction of nonzero products

$$\langle\Phi_j(NJT)\|O(E2)_{p/n}\|\Phi_i'(NJ'T')\rangle$$

in the sum of Eq. (4) together with many amplitudes a_i,a_j' of comparable magnitude and phase relations such that the products

$$a_i a_j'^{*}\langle\Phi_j(NJT)\|O(E2)_{p/n}\|\Phi_i'(NJ'T')\rangle$$

are predominantly of one sign. It is found that these three conditions are satisfied simultaneously for a small but significant subset of the *sd*-shell model $E2$ matrix elements.

III. ROTATIONAL-MODEL ASPECTS

The basic assumption of the collective rotational model of nuclear structure is that the constituents of the nucleus exist in stably deformed shapes and that nuclear energy levels correspond to the allowed states of rotational motion of these shapes. We restrict our consideration here to deformations which are axially symmetric with respect to the z' axis of an internal $x'y'z'$ coordinate system fixed in the nuclear matter. These shapes are

parametrized (to first order in β) as

$$R(\theta')=R_0[1+\beta Y_{20}(\theta',\phi')] , \tag{5}$$

where $R_0=r_0 A^{1/3}$ reproduces the observed rms radius of the nucleus in question and preserves (to second order in β) the volume of the sphere with radius R_0. Geometrically, the parameter β is a measure of the relative difference between the major and minor axes of the spheroid given in Eq. (5). Specifically,

$$\beta=(\tfrac{4}{3})\sqrt{\pi/5}\delta\approx 1.057\delta , \tag{6}$$

where $\delta=\Delta R/R_0$ with $\Delta R=R(\theta'=0)-R(\theta'=\pi/2)$. Such an axially deformed shape has a nonzero intrinsic quadrupole moment Q_0 which is related to the deformation parameters (to second order in β) by

$$Q_0=\sqrt{16\pi/5}\int_0^{2\pi}\int_0^{\pi}\int_0^{R(\theta')} pr'^2 Y_{20}(\theta',\phi') \times r'^2\sin(\theta')dr'd\theta'd\phi'$$

$$=(3/\sqrt{5\pi})ZeR_0^2\beta[1+\tfrac{2}{7}\beta\sqrt{5/\pi}] , \tag{7a}$$

or, in terms of δ,

$$Q_0=(\tfrac{4}{5})ZeR_0^2\delta[1+\tfrac{8}{21}\delta] . \tag{7b}$$

For our present purposes, it is not necessary to know the microscopic origins of the nuclear deformation. In principle, it can be represented by an "intrinsic" state wave function $\chi(\bar{r}')$ which specifies how the nuclear constituents are distributed as a function of the internal coordinates. The total energy of the nucleus is decomposed into the internal energy of the instrinsic state, the energy of the rotational motion of the intrinsic state, and a coupling between these two terms which in the limiting case is assumed to be negligible. In this limit, the total angular momentum J of the system in the laboratory frame, its z component in the laboratory frame, M, and the z component of J along the axis of rotation in the body-fixed frame, K, become good quantum numbers which can be used to label the wave functions $|JKM\rangle$ for the nuclear state (see Refs. 10 or 11 for details).

For each value of K ($K\neq 0$), rotational levels with angular momenta

$$J=|K|,\ |K|+1,\ |K|+2,\ |K|+3,\ldots$$

can be constructed from the intrinsic state $\chi_K(\bar{r}')$, while for $K=0$ we can build sets of rotational levels with, alternatively, $J=0,2,4,6,\ldots$ or $J=1,3,5,7,\ldots$. The energy eigenvalues of the levels within a given band are given[10,11] by the eigenvalue spectrum of a quantum mechanical rotor with total angular momentum J,

$$E(JK)=E(K)+(\hbar^2/2\mathcal{I})[J(J+1) +a(-1)^{J+1/2} \times(J+\tfrac{1}{2})\delta_{K,1/2}] , \tag{8}$$

where[10,11] a is the so called "decoupling parameter," $E(K)$ is the "band-head energy" and $\mathcal{I}$ is the moment of inertia of the intrinsic state about an axis perpendicular to the body-fixed axis of symmetry z'. Except for $K=\frac{1}{2}$, Eq. (8) reduces to the still simpler expression

$$E(JK)=E(K)+(\hbar^2/2\mathcal{I})J(J+1) , \tag{9a}$$

or in terms of the excitation energies of the levels within the band,

$$E_x(J)=E_x(J_B)+(\hbar^2/2\mathcal{I})[J(J+1)-J_B(J_B+1)] , \tag{9b}$$

with J_B representing the total angular momentum of the band head and $E_x(J_B)$ its excitation energy in the nucleus.

The essential step in applying the collective rotational model to electric quadrupole observables is to express the quantities as observed in the laboratory frame of coordinates in terms of the properties of the deformed intrinsic shape, as expressed in the body-fixed coordinate system. The observables are the same as those dealt with in the preceding discussion of the shell-model calculations. As mentioned, we do not attempt to determine explicit expressions for the intrinsic-state wave functions $\chi_K(\bar{r}')$. We assume only that $\langle\chi_K(\bar{r}')|\chi_K(\bar{r}')\rangle$ is unity. In this framework, the electric quadrupole moments and transition strengths are calculated via the standard prescriptions given in Refs. 10 and 11. Specifically, the electric quadrupole moment (for a $K\neq 1$ band) is calculated via the expression[10,11]

$$Q(JK)=\frac{3K^2-J(J+1)}{(J+1)(2J+3)}Q_0(K), \quad (K\neq 1) . \tag{10}$$

and the transition strengths (within a band of given K, i.e., $K_i=K_f=K$) are calculated with the equation

$$B(E2;J_iK\rightarrow J_fK)=M^2(E2;J_iK\rightarrow J_fK)/(2J_i+1) . \tag{11}$$

with

$$|M(E2;J_iK\rightarrow J_fK)|=\sqrt{(5/16\pi)}(2J_i+1)^{1/2}(2J_f+1)^{1/2}\left|\begin{bmatrix} J_f & 2 & J_i \\ -K & 0 & K\end{bmatrix}Q_0(K)+(-1)^{J_i}\begin{bmatrix} J_f & 2 & J_i \\ -K & 2K & K\end{bmatrix}Q_1(K)\right| . \tag{12a}$$

In this equation, $[\cdots]$ is the $3j$ symbol for the angular momentum dependence and for $K\neq\frac{1}{2}$ or 1, the second $3j$ symbol in Eq. (12a) vanishes, giving

$$|M(E2;J_fK\rightarrow J_fK)|=\sqrt{(5/16\pi)}(2J_i+1)^{1/2}(2J_f+1)^{1/2}\left|\begin{bmatrix} J_f & 2 & J_i \\ -K & 0 & K\end{bmatrix}Q_0(K)\right| . \tag{12b}$$

The quadrupole moment $Q(JK)$, and the in-band $E2$ transition strengths $|M(E2; J_iK \rightarrow J_fK)|$, in the laboratory frame can then be calculated from the quadrupole moment of the intrinsic state χ_K, $Q_0(K)$, and the $E2$ intrinsic matrix element connecting the intrinsic state wave functions χ_K and χ_{-K} (not a quadrupole moment), $Q_1(K)$.

In summary, the rotational model as we utilize it here reduces for all values of K other than $K=\frac{1}{2}$ and 1 to the assumption of an intrinsic state χ_K which is characterized by the quantum number K, by a moment of inertia $\mathcal{I}(K)$, and by an intrinsic quadrupole moment $Q_0(K)$, but which is otherwise unspecified. For $K=\frac{1}{2}$, we have the additional two parameters, a and Q_1. Each intrinsic state χ_K can give rise to a "band" of rotational levels $|JKM\rangle$, of ascending values of total angular momentum J, the energies and electric quadrupole matrix elements of which are related to each other by Eqs. (8), (9a), (9b), (10), (12a), and (12b).

IV. ROTATIONAL-MODEL ANALYSIS OF SHELL-MODEL RESULTS

Our goal in the present investigation is to determine the degree to which the shell-model results discussed in Sec. II manifest characteristics similar to the features of the simple rotational model discussed in Sec. III. To this end, we treat the shell model results as "data," e.g., as measured values of E_x and $M(E2)$, and use Eqs. (8), (9a), (9b), (10), (12a), and (12b) to extract from these "data," values of the rotational-model parameters $\hbar^2/2\mathcal{I}$ and $Q_0(K)$. Of course, this process cannot fail to yield values of $\hbar^2/2\mathcal{I}$ and $Q_0(K)$. The question is one of the accuracy with which the deconvolution of the "data" in terms of these simple equations is internally consistent with the underlying concept that all the levels of a "band" are manifestations of a single, stable-deformed, intrinsic shape. That is, do a succession of shell-model energies and $M(E2)$ values yield the same values of $\hbar^2/2\mathcal{I}$ and $Q_0(K)$?

We express the results of our analysis of energies in terms of fits of Eq. (9b) [Eq. (8) for $K=\frac{1}{2}$] to sequences of level excitation energies $E_x(JK)$. The levels fitted are selected first on the basis of being the lowest-energy states available and then, after initial study, upon a more detailed analysis of energy and $E2$ properties in combination. As with real experimental data, the K value of the band is inferred from the J value of the lowest-energy state of the band (except for $K=0, J=$odd, bands), in conjuction with the values of J of the remaining states and their sequence.

The results of the energy-formulae fits are displayed visually by plotting the excitation energies on a vertical scale against the values of $J(J+1)$ plotted on the horizontal scale. Equation (9b) produces straight lines in such plots. In the special case of $K=\frac{1}{2}$, Eq. (8) is operative and the dependence of $E_x(J, K=\frac{1}{2})$ upon J is more complicated. Displays of the individual level energies in comparison with the straight line which yields the rms best fit to the excitation energies of the levels selected as belonging to a band give an indication of the accuracy of such an approximation. In addition to these graphical analyses, we also note the numerical parameters of the fits, namely the slope of the line and the rms deviation value $(\text{rms}=(1/n)\{\sum[E_x(\text{s.m.})-E_x(\text{rot.})]^2\}^{1/2})$.

The values of the electric quadrupole transition matrix elements $|M(E2)|$ and static quadrupole moments Q of the levels of a simple rotational band should all reduce to the same value of $Q_0(K)$. We tabulate the values of $Q_0(K)$ extracted from such shell-model matrix elements under the assumption of a given K value for a putative band and examine them for consistency. The values of Q yield the sign of $Q_0(K)$ as well the magnitude, since for identical initial and final states the arbitrary phases of the wave functions are the same and cancel out. Only the magnitudes of the matrix elements $M(E2)$ between different final and initial states are meaningful.

We give primacy to the consistency of the sign of $Q_0(K)$ in evaluating whether a group of levels can be associated meaningfully with a rotational band, since a stable intrinsic state is the foundation of the simple model and a change in the sign of deformation is evidence of a more profound instability in the intrinsic shape than is a change just in magnitude. Given a constant sign of deformation, the remaining criterion is the degree of constancy in the extracted magnitudes of $Q_0(K)$. We have not formulated a simple numerical criterion for this constancy but, rather, examine each exemplar of a band on a case-by-case basis.

The formula relating electric quadrupole matrix elements Q and $|M(E2)|$ to the intrinsic quadrupole moment $Q_0(K)$ of a band has different features for different K values. The equation relating $Q(JK)/Q_0(K)$ to J. Equation (10) illustrates that the static quadrupole moment Q vanishes for the combination $(K=2, J=3)$. Also, of course, the static quadrupole moments of $J=0$ and $J=\frac{1}{2}$ states are identically zero, as expressed in Eq. (3). As is seen from Eq. (10), the signs of $Q(JK)$ for states of every J value in a band with either $K=0$ or $K=\frac{1}{2}$ are constant and opposite to the sign of the associated intrinsic quadrupole moment $Q_0(K)$. For bands with $K \geq \frac{3}{2}$, however, the sign of $Q(JK)$ relative to that of $Q_0(K)$ will change at some point as the value of J increases. The sign change will occur between $J=\frac{3}{2}$ and $J=\frac{5}{2}$ for $K=\frac{3}{2}$ bands, between $J=\frac{7}{2}$ and $J=\frac{9}{2}$ for $K=\frac{5}{2}$ bands, between $J=4$ and $J=5$ for $K=3$ bands, and, as noted, at $J=3$ for $K=2$ bands.

As with "real" data, there are always ambiguities of one degree or another in selecting which calculated energy levels are "members" of a band and which are not. The ambiguities arise from a combination of deviations from the $J(J+1)$ formula, from variations in the values of $Q_0(K)$ for "in-band" matrix elements and from "large" values for "out-band or cross-band" matrix elements. As the identity of band membership becomes ambiguious we tabulate alternate possibilities of in-band and out-band matrix elements to illustrate the nature of the phenomenon. Our study can be considered as an exploration of how many levels can be attributed to a given

"band" before ambiguity renders the exercise meaningless.

The issue of characterizing the underlying instrinsic state χ_K of a band, and evaluating its constancy, can be addressed by examining the construction of the shell-model wave functions. Watt *et al.*[12,13] have suggested that the occupation numbers of the shell model orbits of the states in a given band should be quasiconstant and should be characteristic of the band. In the full *sd* shell-model space with an ^{16}O inert core, we have

$$\langle 0d_{5/2}\rangle+\langle 1s_{1/2}\rangle+\langle 0d_{3/2}\rangle=A-16\ . \tag{13}$$

Hence, for a given mass number A, only two of these three quantities are independent. A shell-model state can thus be graphically characterized by its position in the $\langle 0d_{5/2}\rangle-\langle 0d_{3/2}\rangle$ occupancy plane. From the numerical values of the occupation numbers of the *sd*-shell wave functions used in this study, we have constructed such plots for various possible bands.

V. RESULTS FOR EVEN-MASS NUCLEI

Data on states which can be characterized as arising from a $K=0$ intrinsic state are simplest to analyze. The sign of the static moment for each state in such a band should be the same and the number of "in-band" $E2$ transitions is limited by the absence of $J\rightarrow J-1$ transitions. We investigate possible $K=0, J=$even, band structures in ^{20}Ne, ^{22}Ne, ^{24}Mg, ^{26}Mg, and ^{28}Si, and a $K=0, J=$odd, band in ^{22}Na. We also investigate a possible $K=2$ band structure in ^{24}Mg and a possible $K=3$ band in ^{22}Na.

A. ^{20}Ne

In the *sd*-shell model space, the low-lying states of ^{20}Ne correspond to two protons and two neutrons coupled to $T=0$. The model wave functions have dimensions for even values of J which range from a maximum of 56, for $J^\pi=2^+$, to a minimum of three, for $J^\pi=8^+$, $J=8$ being the maxium total angular momentum that can be generated with four particles coupled to $T=0$ in the full *sd*-shell model space. The excitation energies of the first 0^+, 2^+, 4^+, 6^+, and 8^+ states calculated for ^{20}Ne are shown plotted versus a $J(J+1)$ spacing in Fig. 1. The least-squares fit of the straight line [Eq. (9b)] to these points is given by $E_x(\text{keV})=186J(J+1)$, with an rms deviation of 530 keV. We see from Fig. 1 that the energies of the 2^+, 4^+, and 6^+ states lie above this best-fit line and that of the 8^+ state noticeably below it.

The electric quadrupole matrix elements calculated from these model wave functions of ^{20}Ne, and the values of $Q_0(K=0)$ extracted from them under the assumption that they are members of a $K=0$ rotational band, are presented in Table I. The value of $Q_0(K=0)$ extracted from the average of the values of the $2^+\leftrightarrow 0^+$ and $4^+\leftrightarrow 2^+$ transition matrix elements and the 2^+ and 4^+ static moments, is $+50.9\pm 1.9$ efm^2. The positive sign of $Q_0(K=0)$ is inferred from the negative signs calculated

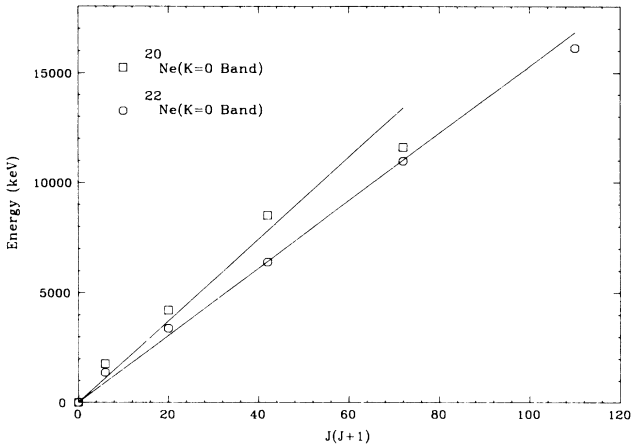

FIG. 1. Plot of E_x vs $J(J+1)$ for the suggested $K=0$ band in ^{20}Ne (squares) and the suggested $K=0$ band in ^{22}Ne (circles).

for the 2^+ and 4^+ static moments. This value of $Q_0(K=0)$ corresponds to a large prolate deformation of the intrinsic shape [$\delta=+0.51$ from Eq. (7b)]. The values of $Q_0(K=0)$ extracted from the static moments of the 6^+ and 8^+ states are also positive, indicating a stable prolate deformation throughout the sequence, but their magnitudes are smaller than those extracted from the states of lower J, the value for $J=8$ by a factor of about 0.8. For values of J equal to and greater than 2, the values of $Q_0(K=0)$ extracted from the transition matrix elements between states of J and $J+2$ are smaller than the $Q_0(K=0)$ values extracted from the separate static moments $Q(J)$ and $Q(J+2)$ for the same two states.

The occupation numbers (Fig. 2) for the 0^+ and 2^+ states are very similar. The $0d_{5/2}$ occupancies in the 4^+ and 6^+ states are larger than the 0^+ and 2^+ values by 0.4 and 0.6 units, respectively, these increases coming at the expense of the $1s_{1/2}$ occupancy. The $0d_{5/2}$ occupation of the 8^+ state is 1.1 units greater than for 0^+ and 2^+, and its $1s_{1/2}$ occupancy is zero. These changes of occupancy among the higher-spin members of the presumed band occur as more and more configurations which involve $s_{1/2}$ and $d_{3/2}$ terms fail to be able to generate the requisite total angular momenta for the four-particle states. The changes are seen to correlate with discernable, but still relatively small, effects upon the calculated energies and $E2$ properties of these states.

B. ^{22}Ne

The dimensions for model states of $A=22$, $T=1$, and even values of J range from a maximum of 525 for $J^\pi=2^+$ to a minimum of six for $J^\pi=10^+$. The latter value is the maximum value of total angular momentum which can be constructed for this system of six active particles in the full *sd*-shell model space. The energies calculated for the lowest 0^+, 2^+, 4^+, 6^+, 8^+, and 10^+ states of ^{22}Ne are shown plotted against the $J(J+1)$ spacing in Fig. 1. The least-squares straight-line fit to these data is given by $E_x(\text{keV})=153\,J(J+1)$, with a rms

TABLE I. Values of calculated electric quadrupole matrix elements $M(E2; J_i \leftrightarrow J_f)$ and $Q(J_i)$ for $T=0$ states in ^{20}Ne and ^{28}Si and $T=1$ states in ^{22}Ne and ^{26}Mg, together with values of Q_0 extracted from these matrix elements and from corresponding experimental data under the assumption that the states are members of $K=0$ rotational bands. The values quoted in the Q, $|M(E2)|$ column are $|M(E2)|$ when different states are involved and are Q when the initial and final states are identical. States whose J values are not subscripted are the first occurring states of the respective J-T values. The units are efm^2.

States	Q, $\|M(E2)\|$	Q_0	Q_0(exp)[a]
	^{20}Ne ($K=0$)		
$2^+ \leftrightarrow 0^+$	16.4	52.1	58.0±1.7
$Q(2^+)$	−14.9	+52.3	+80.7±10.5
$4^+ \leftrightarrow 2^+$	24.1	47.6	50.2±2.4
$Q(4^+)$	−18.8	+51.6	
$6^+ \leftrightarrow 4^+$	25.5	39.9	
$Q(6^+)$	−18.8	+47.1	
$8^+ \leftrightarrow 6^+$	23.5	31.5	
$Q(8^+)$	−17.6	+41.8	
	^{22}Ne ($K=0$)		
$2^+ \leftrightarrow 0^+$	15.2	48.1	47.8±0.4
$Q(2^+)$	−13.6	+47.5	+66.4±14.0
$4^+ \leftrightarrow 2$	23.7	46.9	47.6±0.4
$Q(4^+)$	−17.0	+46.8	
$6^+ \leftrightarrow 4^+$	25.7	40.3	40.1±2.2
$Q(6^+)$	−18.5	+46.3	
$8^+ \leftrightarrow 6^+$	20.2	27.0	
$Q(8^+)$	−14.9	+35.3	
$10^+ \leftrightarrow 8^+$	11.5	13.7	
$Q(10^+)$	−14.5	+33.2	
	^{28}Si ($K=0$)		
$2^+ \leftrightarrow 0^+$	18.5	−58.7	−57.4±0.8
$Q(2^+)$	+17.1	−59.9	−56.0±10.5
$4^+ \leftrightarrow 2^+$	29.6	−58.4	−49.6±2.4
$Q(4^+)$	+21.3	−58.5	
$6^+ \leftrightarrow 4^+$	33.1	−51.9	−39.4±5.5
$Q(6^+)$	+26.2	−65.6	
$8^+ \leftrightarrow 6^+$	32.3	−43.3	
$Q(8^+)$	+24.5	−58.3	
$10^+ \leftrightarrow 8^+$	32.2	−38.3	
$Q(10^+)$	+25.7	−59.0	
$Q(10_2^+)$	−10.5	+24.1	
$12^+ \leftrightarrow 10^+$	24.8	−26.8	
$Q(12^+)$	+28.8	−64.7	
$Q(12_2^+)$	−21.7	+48.7	
$Q(12_3^+)$	4.88	−11.0	
$Q(12_4^+)$	1.76	−3.96	
$Q(12_5^+)$	−2.38	+5.35	
$14^+ \leftrightarrow 12^+$	0.37	−0.37	
$Q(14^+)$	0	0	
	^{26}Mg ($K=0$)		
$2^+ \leftrightarrow 0^+$	17.3	55.0	56.7±1.2
$2_2^+ \leftrightarrow 0^+$	3.00	9.54	11.9±1.2
$Q(2^+)$	−12.0	+42.1	+45.6±10.5
$Q(2_2^+)$	+12.3	−43.2	
$4^+ \leftrightarrow 2^+$	14.3	28.2	27.6±0.9
$4^+ \leftrightarrow 2_2^+$	6.69	13.2	
$4_2^+ \leftrightarrow 2^+$	19.5	38.5	46.8±4.3
$4_2^+ \leftrightarrow 2_2^+$	9.39	18.5	33.4±7.3
$Q(4^+)$	+2.31	−6.47	
$Q(4_2^+)$	+0.075	−0.21	
$6_2^+ \leftrightarrow 4^+$	7.32	11.5	
$6_2^+ \leftrightarrow 4_2^+$	17.2	27.0	
$Q(6^+)$	−1.22	+3.06	
$Q(6_2^+)$	+14.4	−36.1	
$8_2^+ \leftrightarrow 6_2^+$	12.0	16.1	
$Q(8_2^+)$	18.0	−42.8	
$10^+ \leftrightarrow 8_2^+$	11.3	13.4	
$Q(10^+)$	21.8	−50.1	
$10_2^+ \leftrightarrow 8_2^+$	1.20	1.43	
$Q(10_2^+)$	−3.37	+7.75	
$10_3^+ \leftrightarrow 8_2^+$	0.59	0.70	
$Q(10_3^+)$	−17.3	+39.8	
$10_4^+ \leftrightarrow 8_2^+$	4.54	5.40	
$Q(10_4^+)$	0.15	−0.35	
$12^+ \leftrightarrow 10^+$	2.83	3.06	
$12^+ \leftrightarrow 10_2^+$	12.9	13.9	
$12^+ \leftrightarrow 10_3^+$	13.3	14.4	
$12^+ \leftrightarrow 10_4^+$	4.7	5.08	
$Q(12^+)$	−12.4	+27.9	
$12_2^+ \leftrightarrow 10^+$	0.09	0.10	
$12_2^+ \leftrightarrow 10_2^+$	1.85	2.00	
$12_2^+ \leftrightarrow 10_3^+$	12.9	13.9	
$12_2^+ \leftrightarrow 10_4^+$	3.57	3.86	
$Q(12_2^+)$	−6.26	+14.1	
$12_3^+ \leftrightarrow 10^+$	3.33	3.60	
$12_3^+ \leftrightarrow 10_2^+$	4.08	4.41	
$12_3^+ \leftrightarrow 10_3^+$	1.54	1.66	
$12_3^+ \leftrightarrow 10_4^+$	12.1	13.1	
$Q(12_3^+)$	−9.15	+20.6	
$Q(12_4^+)$	−14.1	+31.7	

[a]Taken from Ref. 7.

deviation of 179 keV. The energy points are distributed about the line similarly to those of ^{20}Ne, but the scatter is much smaller, as is reflected by the smaller value of the rms deviation. The only significant excursions are for the 2^+ state (slightly too high) and the 10^+ state (slightly too low).

The values of the electric quadrupole matrix elements calculated for these model states of ^{22}Ne and the values of $Q_0(K=0)$ extracted from them under the assumption that they are members of $K=0$ rotational band are presented in Table I. All values of the static moments $Q(J)$ are negative, corresponding to all positive values of $Q_0(K=0)$ and a stable prolate deformation. This is consistent with what was found for the ^{20}Ne wave functions. The value of $Q_0(K=0)$ extracted from the average of the values from the 2^+ and 4^+ static moments and the $2^+ \leftrightarrow 0^+$ and $4^+ \leftrightarrow 2^+$ transition matrix elements is $+47.3 \pm 0.5$ efm^2 ($\delta = +0.44$). The value of $Q_0(K=0)$ from the static moment of the 6^+ state is consistent with this value, while those from the 8^+ and 10^+ states are

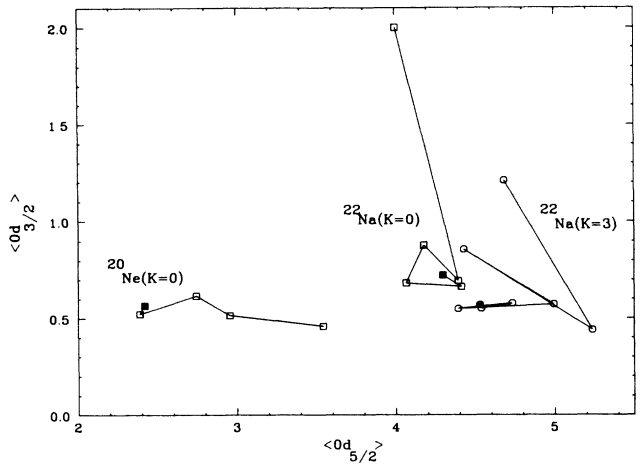

FIG. 2. Occupancy diagram for states in the suggested rotational bands in ^{20}Ne and ^{22}Na. The solid point for each nucleus represents the band head and the points are connected in order of increasing J values.

significantly smaller. As for ^{20}Ne, the $Q_0(K=0)$ values extracted from the transition matrix elements between states of J and $J+2$ are smaller than those extracted from the bracketing static moments for higher values of J.

The occupancies of the $0d_{5/2}$ orbit (Fig. 3) are quite stable throughout the range of J values, the only fluctuation being the 0.4 unit jump for $J=8$. The $1s_{1/2}$ occupancies decrease noticeably for $J=8$ and $J=10$, particularly for $J=10$, where most of the configurations involving this orbit are unable to generate the required angular momentum. As is evident from Fig. 3, the clustering of the $J=0-6$ points in the ^{22}Ne occupancy diagram is much tighter than for the corresponding points of ^{20}Ne. Taken together, the energies, the quadrupole matrix elements

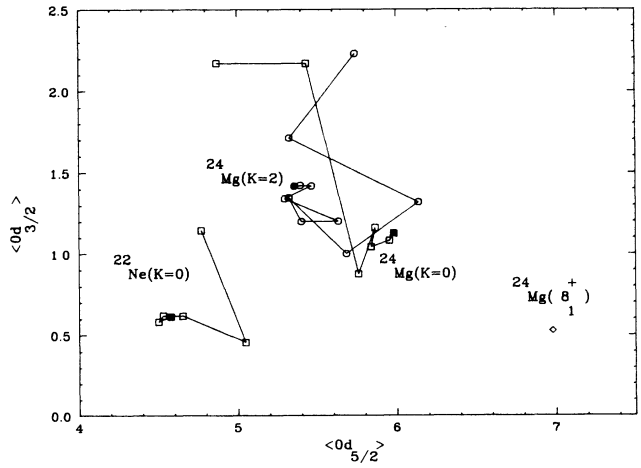

FIG. 3. Occupancy diagram for states in the sugggested rotational bands in ^{22}Ne and ^{24}Mg. Also included are the occupation numbers for the yrast 8^+ state in ^{24}Mg. The solid point for each nucleus represents the band head and the points are connected in order of increasing J values.

and the occupation numbers all are suggestive of a stable intrinsic state generating a "$K=0$ band" in ^{22}Ne.

C. ^{28}Si

The model wave functions for ^{28}Si have 12 particles (or 12 holes) in the *sd* shell. The dimensions for even values of J range from 3793 for the $J^\pi=4^+$ spin to one for $J^\pi=14^+$, the maximum total angular momentum for 12 particles coupled to $T=0$ in the *sd* shell. The calculated energies of the lowest occuring states in ^{28}Si with even values of J from 0 through 14 are shown plotted against a $J(J+1)$ spacing in Fig. 4(a). The least-squares straight-line fit to these points is given by $E_x(\text{KeV})=192J(J+1)$, with an rms deviation of 604 keV. The most significant excursions from the line occur at $J=12$, where the shell-model eigenvalue is roughly 3 MeV below the line and at $J=14$ which is comparably too high.

The calculated $E2$ static moments and transition matrix elements of these states of ^{28}Si, and the values of $Q_0(K=0)$ extracted from them, are shown in Table I. The signs of the static moments $Q(J)$ are all positive, leading to a negative value of $Q_0(K=0)$ and a consistent oblate deformation. The value of $Q_0(K=0)$, taken from averages of the 2^+ and 4^+ static moments and the $2^+\leftrightarrow 0^+$ and $4^+\leftrightarrow 2^+$ transition matrix elements, is -58.9 ± 0.6 efm^2, and corresponds to $\delta=-0.49$. The values of $Q_0(K=0)$ extracted from the static moments do not show the decrease in magnitude with increasing J that was found in ^{20}Ne and ^{22}Ne, the values for 6^+, 8^+,

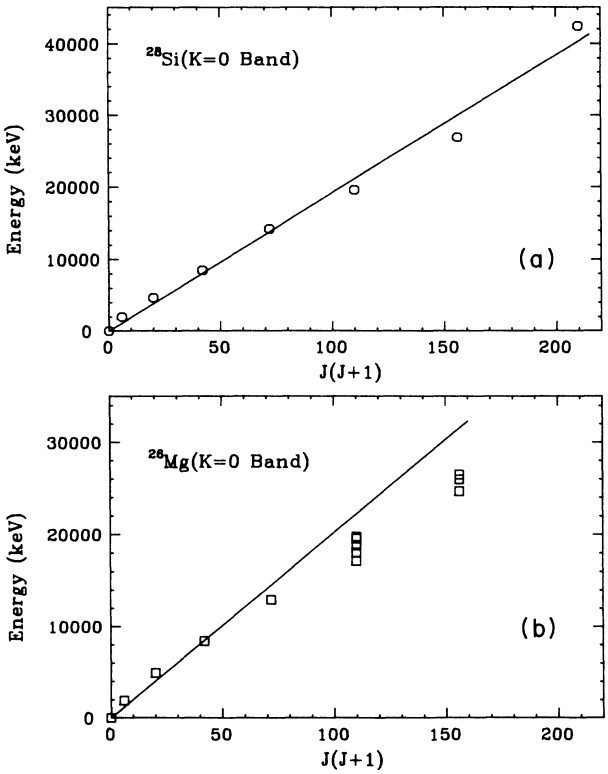

FIG. 4. Plot of E_x vs $J(J+1)$ for the suggested $K=0$ band in (a) ^{28}Si and (b) ^{26}Mg.

10^+, and 12^+ being -66, -58, -59, and -65 efm^2, respectively. For values of J higher than four, the values of $Q_0(K=0)$ extracted from the transition matrix elements between states of J and $J+2$ are smaller in magnitude than the values from the static moments of the bracketing states, behavior which is consistent with that found in ^{20}Ne and ^{22}Ne.

As mentioned [see Fig. 4(a)], the excitation energy of the yrast 12^+ level in ^{28}Si falls below the best-fit $J(J+1)$ line by more than 3 MeV in energy. There exist four higher-lying 12^+ shell-model states in the ^{28}Si system whose energies are within 2.4–0.8 MeV of the best-fit $J(J+1)$ line, suggesting (at least on the basis of energy) that one of these higher 12^+ states should belong to the $K=0$ ground-state band. To address this possibility, we show in Table I the calculated values of $Q_0(K=0)$ extracted from the quadrupole moments of these states. In all cases, these values of $Q_0(K=0)$ are either much too small in magnitude or of the wrong sign. Hence, we conclude that the lowest energy 12^+ level is the best candidate for membership in the ground-state $K=0$ band. In the ^{29}Si system, only one 14^+ level is possible. Its model wave function is the pure $(0d_{5/2})^6$-$(1s_{1/2})^2$-$(0d_{3/2})^4$ configuration and so, by the selection rule[14] that $E2$ matrix elements between states of the same seniority vanish for half-filled shells, its quadrupole moment must be zero. The small value of the $12^+ \leftrightarrow 14^+$ $E2$ transition strength results from the fact that the three largest components (17.3%, 13.7%, and 10.7%) of the 12^+ wave function contain eight particles in the $0d_{5/2}$ subshell and hence cannot be connected to the 14^+ wave function by the one-body $E2$ operator.

The occupation numbers of the sd-shell orbits for ^{28}Si states of the presumed $K=0$ ground-state band (Fig. 5) show quite a different trend from those observed in ^{20}Ne and ^{22}Ne. The $0d_{5/2}$ occupancy for the 0^+ state is much larger (by 0.8 units) than for any of the other states, and its value decreases steadily from $J^\pi=2^+$ to 12^+, then

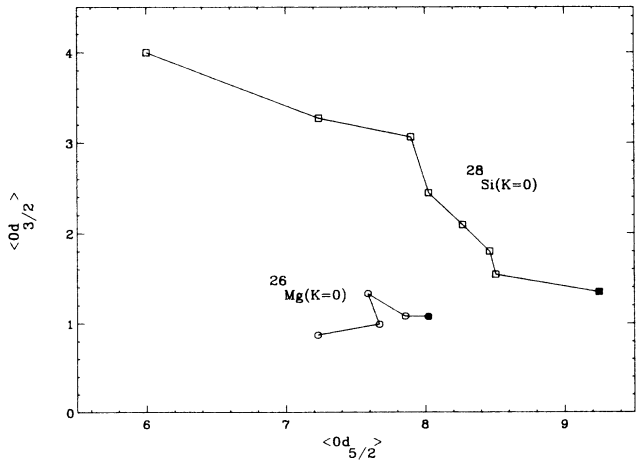

FIG. 5. Occupancy diagram for states in the suggested rotational bands in ^{26}Mg and ^{28}Si. The solid point for each nucleus represents the band head and the points are connected in order of increasing J values.

makes another major decrease in going to the $J^\pi=14^+$ state. The change in occupancy between the 0^+ and 2^+ states reflects the filling of the $0d_{5/2}$ orbit with 12 particles. Twelve particles can occupy the $0d_{5/2}$ orbit only when coupled to $J=0$. This configuration dominates (19.7%) the ground-state model wave function and this thereby enhances its $0d_{5/2}$ occupancy relative to all other states. The trends for the higher-spin states are understood better in terms of hole, rather than particle, occupancies. The decrease in the $0d_{5/2}$ occupancies for higher spin states between $J=2$ and 10 can be understood in the same fashion as the trends observed for the ^{20}Ne and ^{22}Ne examples, namely as in transfering degrees of freedom from the $1s_{1/2}$ and $0d_{3/2}$ to the $0d_{5/2}$ orbit so as to satisfy the need for additional net angular momentum. However, in the present 12-particle example, additional Pauli effects come into play, since beyond $J=10$, the $0d_{5/2}$ orbit becomes saturated and occupancy must return to the lower-spin orbits. In this nucleus the electric quadrupole data suggest a $K=0$ band originating in a well-defined oblate intrinsic shape. However, there are significant fluctuations in the energy systematics and in the occupation numbers of these states over the entire range of J values. These contrasting results leave the issue of what defines a "band" more ambiguous.

D. ^{26}Mg

The model states for the system of ten sd-shell particles coupled to $T=1$ range from $J=0$ to 12 and have dimensionalities ranging from a maximum of 5028 for $J^\pi=4^+$ to a minimum of 30 for $J^\pi=12^+$. Eigenvalues of even-spin states are shown plotted against $J(J+1)$ in Fig. 4(b). We initially assume, as discussed in the following paragraphs, that there is a $K=0$ ground-state band which consists of the 0^+, 2^+, 4_2^+, 6_2^+, and 8_2^+ levels. The least-squares straight-line fit to only these five points is given by $E_x(\text{keV})=202\,J(J+1)$, with an rms deviation of 489 keV. An extrapolation of this best-fit line leads, however, to ambiguities about the identity of the 10^+ and 12^+ levels that should belong to this putative band, the lowest-energy states of these spins falling well below the projected line.

The values of the calculated $E2$ static moments and transition matrix elements of these states (along with many other states in the ^{26}Mg system), and the values of $Q_0(0)$ extracted from them, are presented in Table I. It can be seen immediately that the regularities observed in the results for $A=20$, 22, and 28 are not present in these ^{26}Mg numbers. The $Q_0(K=0)$ values extracted from the static moments change from $+42$ efm^2 to zero, to -36 efm^2, to -43 efm^2 in progressing from $J=2$ to 8. Alternate choices for membership in the $K=0$ band create an even greater scatter of magnitudes and signs. The values of $Q_0(K=0)$ derived from the transition matrix elements are quite different, sometimes strikingly so, from those derived from the bracketing static moments.

If the information upon which to base the decision consisted only of the transition matrix elements, it would be possible, on the basis of their extracted $Q_0(K=0)$ values, to postulate that the above levels formed a $K=0$

band, even if a rather significantly perturbed one. Such an interpretation was made, on the basis of these calculations and corresponding experimental data, in Ref. 15. However, the values of $Q_0(K=0)$ derived from the static moments of these states show that there does not exist in ^{26}Mg a set of states which can be characterized as a rotational band in the same sense that the sets of levels in ^{20}Ne, ^{22}Ne, and ^{28}Si can be simply so characterized.

The occupation numbers for the states of ^{26}Mg in the initially assumed band are plotted in Fig. 5. Apart from the 0^+ and 2^+ levels, the $0d_{5/2}$ occupancies show variations of 0.3–0.5 units. These variations are not larger than what were found in ^{20}Ne and ^{22}Ne, even though the energies and the electric-quadrupole properties of these states in ^{26}Mg suggest little intrinsic-band structure.

E. $K=0$, $J=$odd, and $K=3$ bands in ^{22}Na

The states of three active protons and three active neutrons coupled to $T=0$ correspond in the *sd*-shell model to levels of ^{22}Na. In the full *sd*-shell basis space the state dimensions range from a maximum of 366 for $J=3$ to a minimum of one for $J=11$, the maximum value for the total angular momentum which can be generated for this system in the basis. Some eigenvalues calculated for these states are shown plotted against the $J(J+1)$ spacing in Fig. 6(a). Two straight lines are shown fitted to these points, one to the energies of a presumed $K=3$ band consisting of the $J^\pi=3^+$, 4^+, 5^+, 6^+, 7^+, 8^+, 9^+, and 10^+ states, the other to energies of a presumed J odd, $K=0$ band consisting of the $J^\pi=1^+$, 3_2^+, 5_2^+, 7_2^+, 9_2^+, and 11^+ states. The equation for the $K=3$ line is $E_x(\text{keV})=135J(J+1)-1620$ and has an rms deviation of 389 keV. The equation for the $K=0$ line is $E_x(\text{keV})=138J(J+1)+114$ and has an rms deviation of 120 keV. Both lines are essentially parallel, reflecting that the two bands have almost identical moments of inertia. Both of these bands could incorporate a $J^\pi=11^+$ state, but there is only one such state in the *sd* shell-model space. On the basis of its energy it would appear most appropriate to associate the existing state with the $K=0$ band. However, we have seen in the previous examples that the energy of the highest-spin states in the various shell-model systems, with their very small dimensionalities, typically are not very consistent with the trends from the lower-spin states.

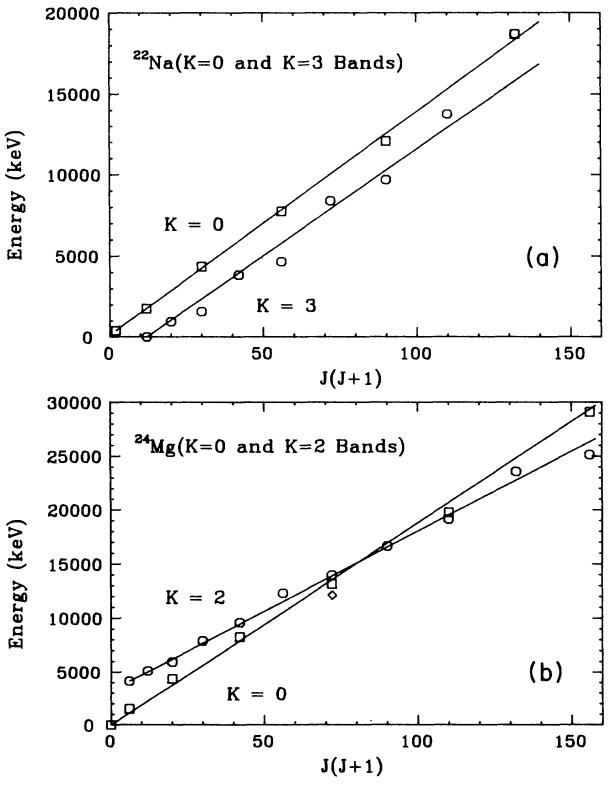

FIG. 6. (a) Plot of E_x vs $J(J+1)$ for the suggested $K=0$, J odd (squares), and $K=3$ (circles) bands in ^{22}Na. (b) Plot of E_x vs $J(J+1)$ for the suggested $K=0$ (squares) and $K=2$ (circles) bands in ^{24}Mg.

The $E2$ matrix elements calculated from the wave functions of these states of ^{22}Na, together with the values of $Q_0(K=3)$ and $Q_0(K=0)$ extracted from them under the assumptions that they are members of $K=3$ and $K=0$ bands as noted, are presented in Table II. The relationship between the signs of $Q(J)$ and $Q_0(K=3)$ dictated by Eq. (10) yields the same sign for the static quadrupole moments $Q(J)$ and the intrinsic quadrupole moment $Q_0(K=3)$ of the states with $J=3$ and 4, while for states with $J\geq 5$, $Q(J)$, and $Q_0(K=3)$ have opposite signs. For $J=5$ states the magnitude of $Q_0(K=3)$ is 26 times that of $Q(J)$. The calculated values of the static moments $Q(J)$ of the presumed $K=3$ states of ^{22}Na yield positive signs for each value of $Q_0(K=3)$, corresponding to a stable prolate deformation of the intrinsic shape. The magnitude of $Q_0(K=3)$ obtained from the average of the values from the 3^+ and 4^+ static moments and the $4^+\leftrightarrow 3^+$ transition matrix element is $+53.4\pm2.7$ efm^2, which corresponds to a value of $\delta=+0.46$. The values of $Q_0(K=3)$ extracted from the static moments of the states of higher angular momentum are about 0.8 of this value, and the $Q_0(K=3)$ values extracted from the transition matrix elements between the higher-spin states are about 0.6 of this "band-head" value.

The value of $Q_0(K=3)$ extracted for the $J=5$ state is exceptional because of the large ratio of $Q_0(K=3)$ to Q yielded by Eq. (10). The value calculated for the static moment Q of the $J=5$ state (-0.7 efm^2) is very small relative to the typical magnitude of $E2$ matrix elements calculated in the present shell-model context and a negligible variation (≈ 1 efm^2) in this value would put the extracted value of $Q_0(K=3)$ for the 5^+ state in line with the other values.

If we now focus on the $E2$ matrix elements for the $K=0$, $J=$odd band, we find that $Q(J)$ and $Q_0(K=0)$ have opposite signs for all J in accordance with Eq. (10). The positive signs for each value of $Q_0(K=0)$ correspond to a stable prolate deformation of the intrinsic shape. The magnitude of $Q_0(K=0)$ obtained from the average of the values from the 1^+ and 3_2^+ static moments and the $1^+\leftrightarrow 3_2^+$ transition matrix element is $+52.7\pm0.8$ efm^2,

TABLE II. Values of calculated electric quadrupole matrix elements $M(E2;J_i \leftrightarrow J_f)$ and $Q(J_i)$ for $T=0$ states in ^{22}Na, together with values of Q_0 extracted from these matrix elements and from corresponding experimental data under the assumption that the states, variously, are members of $K=0$ and $K=3$ rotational bands. The values quoted in the Q, $|M(E2)|$ column are $M(E2)$ when different states J_i and J_f are involved and are Q when the initial and final states J_i are identical. States whose J values are not subscripted are the first occuring states of the respective J-T values. The units are efm^2.

States	Q, $\|M(E2)\|$	Q_0	Q_0(exp)[a]
	^{22}Na ($K=0$)		
$Q(1^+)$	−10.6	+53.2	
$3_2^+ \leftrightarrow 1^+$	21.8	51.6	50.0±2.2
$Q(3_2^+)$	−17.8	53.3	
$5_2^+ \leftrightarrow 3_2^+$	25.4	44.1	39.4±6.6
$Q(5_2^+)$	−20.1	+52.2	
$7_2^+ \leftrightarrow 5_2^+$	28.4	40.8	
$Q(7_2^+)$	−20.9	+50.7	
$9_2^+ \leftrightarrow 7_2^+$	18.0	22.6	
$Q(9_2^+)$	−16.2	+37.8	
$11^+ \leftrightarrow 9_2^+$	6.40	7.24	
$Q(11^+)$	−16.9	+48.3	
	^{22}Na ($K=3$)		
$Q(3^+)$	22.1	+53.0	
$4^+ \leftrightarrow 3^+$	28.1	50.3	50.6±0.7
$Q(4^+)$	7.23	+56.8	
$5^+ \leftrightarrow 3^+$	14.7	48.1	47.0±0.9
$5^+ \leftrightarrow 4^+$	29.0	48.4	49.9±1.7
$Q(5^+)$	−0.702	+18.3	
$6^+ \leftrightarrow 4^+$	19.9	45.0	43.5±4.1
$6^+ \leftrightarrow 5^+$	26.8	45.6	42.1±4.3
$Q(6^+)$	−6.60	+46.2	
$7^+ \leftrightarrow 5^+$	23.3	42.8	41.4±6.2
$7^+ \leftrightarrow 6^+$	26.0	46.0	
$Q(7^+)$	−7.9	+37.0	
$8^+ \leftrightarrow 6^+$	22.7	36.4	
$8^+ \leftrightarrow 7^+$	22.3	41.3	
$Q(8^+)$	−12.7	+48.2	
$9^+ \leftrightarrow 7^+$	20.4	29.4	
$9^+ \leftrightarrow 8^+$	13.7	26.4	
$Q(9^+)$	−12.8	+42.8	
$10^+ \leftrightarrow 8^+$	22.7	30.1	
$10^+ \leftrightarrow 9^+$	17.2	34.6	
$Q(10^+)$	−14.1	+42.9	
$11^+ \leftrightarrow 9^+$	0.003	0.004	
$11^+ \leftrightarrow 10^+$	14.2	29.8	
$Q(11^+)$	−16.9	+48.3	

[a]Taken from Ref. 7.

which corresponds to a value of $\delta = +0.46$. This deformation is essentially identical to that of the $K=3$ band. This is consistent with the parallelism of the best-fit excitation energy lines of Fig. 6(a), since the slopes of these lines are related to the momenta of inertia of the intrinsic shapes and hence should be equal for identical shapes. In contrast to the ground-state $K=0$, $J=$even bands, the values of $Q_0(K=0)$ extracted from the static moments of the states of higher angular momentum in this band (excluding the 9_2^+ level) are about 0.95 of the "band-head" value, and the $Q_0(K=0)$ values extracted from the transition matrix elements between the higher-spin states (again excluding the 9_2^+ level) are about 0.8 of this "band-head" value.

As noted earlier, there is only one way to construct a state with spin 11^+ from *sd*-shell orbits in this $A=22$, $T=0$ system. The value of $Q_0(K)$ extracted from the calculated quadrupole moment Q of the 11^+ state is consistent in both sign and magnitude with the value of either the extant $Q_0(K=3)$ or $Q_0(K=0)$ value. However, the energy of this level favors associating it with the $K=0$ band and, although both the $11^+ \leftrightarrow 9^+$ and the $11^+ \leftrightarrow 9_2^+$ $E2$ transitions are small compared to other $E2$ "in-band" transitions in the $K=0$ ad $K=3$ bands, the $11^+ \leftrightarrow 9_2^+$ $E2$ transition is three orders of magnitude larger than that of the $11^+ \leftrightarrow 9^+$ $E2$ transition. Thus, it would appear that the unique 11^+ *sd*-shell model level in ^{22}Na should be associated with the $K=0$, $J=$odd band.

The $0d_{5/2}$ occupation numbers for these two bands (Fig. 2) show that they are nicely separated in the occupancy plot, with the $0d_{5/2}$ occupation of the $K=3$ band being on average greater than that of the $K=0$ band. Excluding the 11^+ level, the members of the $K=0$, $J=$odd band have $0d_{5/2}$ occupation numbers which scatter by about 0.25 units from the mean. The $0d_{5/2}$ occupancies for states in the $K=3$ band show a larger variation, particularly for the 8^+ and 9^+ states. Taking energies, quadrupole matrix elements and occupation numbers all into account, the states of each of these two "bands" in ^{22}Na appear, similarly to what was found for an analogous group of states in ^{22}Ne, to be closely related to other members of the band when viewed through the rotational-model analysis.

The question of how distinct the two bands of shell-model states in ^{22}Na are, can also be addressed by calculating the $E2$ matrix elements between a state in one band and a state in the other. In the limit of the simple rotational model, these $E2$ matrix elements should be zero. Values of $E2$ matrix elements between the levels in the nominal $K=0$ band and the levels in the nominal $K=3$ band (i.e., cross-band transitions) are shown in Table III. The values are not zero but are, on the average, significantly smaller (a factor of 3–4) than the "in-band" $E2$ matrix elements. The only "large" $E2$ transition rates occur for the $9_2^+ \leftrightarrow 9^+$ and $10^+ \leftrightarrow 11^+$ processes. The large $M(E2;10^+ \leftrightarrow 11^+)$ element, as mentioned already, is an indication that the unique 11^+ shell-model state is shared between the $K=0$ and $K=3$ rotational bands, with most of the state belonging to the $K=0$ band.

F. $K=0$ and $K=2$ bands in ^{24}Mg

The model wave functions for ^{24}Mg have dimensions ranging from a maximum of 1311 for $J^\pi = 4^+$ to a minimum of six, for $J^\pi = 12^+$, the maxium total angular momentum allowed for eight particles in *sd*-shell orbits coupled to $T=0$. The energies of $T=0$ states with J from 0 through 12 are shown plotted versus a $J(J+1)$ spacing in Fig. 6(b). Two different straight lines are fitted to sets of these points, one to the set 0^+, 2^+, 4^+, 6^+, 8_2^+, 10_2^+, and 12_2^+, the other to the set 2_2^+, 3^+, 4_2^+, 5^+, 6_2^+, +, 8_3^+, 9^+, 10^+, 11^+, and 12^+. The equation for the best fit to

TABLE III. Calculated and experimental cross-band $E2$ transitions in ^{22}Na and ^{24}Mg. (Units are in efm^2.)

^{22}Na States	$\lvert M(E2)\rvert_{\text{s.m.}}$	$\lvert M(E2)\rvert_{\text{exp}}$[a]	^{24}Mg States	$\lvert M(E2)\rvert_{\text{s.m.}}$	$\lvert M(E2)\rvert_{\text{exp}}$[a]
$3^+\leftrightarrow 1^+$	0.517	0.32±0.01	$2^+\leftrightarrow 2_2^+$	8.71	7.43±0.34
$3^+\leftrightarrow 3_2^+$	0.572	<1.21	$3^+\leftrightarrow 2^+$	8.37	8.16±0.38
$4^+\leftrightarrow 3_2^+$	1.16	<4.55	$4_2^+\leftrightarrow 2^+$	5.30	
$5^+\leftrightarrow 3_2^+$	2.89		$4^+\leftrightarrow 3^+$	8.23	
$5_2^+\leftrightarrow 3^+$	2.31		$4_2^+\leftrightarrow 4^+$	10.6	
$5_2^+\leftrightarrow 4^+$	3.78		$5^+\leftrightarrow 4^+$	9.18	11.02±0.93
$5_2^+\leftrightarrow 5^+$	5.20		$6_2^+\leftrightarrow 4^+$	1.43	4.50±1.44
$6^+\leftrightarrow 5_2^+$	2.59		$6^+\leftrightarrow 5^+$	16.5	
$7^+\leftrightarrow 5_2^+$	3.17		$6_2^+\leftrightarrow 6^+$	11.0	
$7_2^+\leftrightarrow 5^+$	0.915		$7^+\leftrightarrow 6^+$	4.90	
$7_2^+\leftrightarrow 6^+$	4.49		$8_3^+\leftrightarrow 6^+$	17.8	
$7_2^+\leftrightarrow 7^+$	5.29		$8_2^+\leftrightarrow 7^+$	9.58	
$8^+\leftrightarrow 7_2^+$	2.45		$8_3^+\leftrightarrow 8_2^+$	10.3	
$9^+\leftrightarrow 7_2^+$	8.44		$9^+\leftrightarrow 8_2^+$	3.41	
$9_2^+\leftrightarrow 7^+$	3.26		$10^+\leftrightarrow 8_2^+$	20.7	
$9_2^+\leftrightarrow 8^+$	0.673		$10_2^+\leftrightarrow 9^+$	5.41	
$9_2^+\leftrightarrow 9^+$	16.1		$10_2^+\leftrightarrow 10^+$	3.28	
$10^+\leftrightarrow 9_2^+$	3.82		$11^+\leftrightarrow 10_2^+$	15.5	
$11^+\leftrightarrow 9^+$	0.003		$12^+\leftrightarrow 10_2^+$	27.9	
$11^+\leftrightarrow 9_2^+$	6.40		$12_2^+\leftrightarrow 11^+$	7.80	
$11^+\leftrightarrow 10^+$	14.2		$12_2^+\leftrightarrow 12^+$	9.48	

[a]Taken from Ref. 7.

the first set, assumed to correspond to the members of a $K=0$ band, is given by $E_x(\text{keV})=188\,J(J+1)$, with an rms deviation of 216 keV. The equation for the second set of energies, assumed to correspond to members of a $K=2$ band, is

$$E_x(\text{keV})=148J(J+1)+3234\ ,$$

with an rms deviation of 257 keV. As seen from Fig. 6(b), the lines cross between $J^\pi=8^+$ and $J^\pi=10^+$. In addition, the lowest energy 8^+ state is not included as a member of either assumed band.

An interesting property of the entire geneology[6,16,17] of the empirical Wildenthal Hamiltonians, in which they differ from the Kuo-Brown[18] and other theoretically derived Hamiltonians, is that they predict the lowest 8^+ state in ^{24}Mg to be a "spherical" or "$0d_{5/2}$ condensate" state, not the member of either the "ground-state" $K=0$ or the "excited-state" $K=2$ rotational band. Considerable experimental evidence[19] has been obtained subsequent to these predictions that such a "spherical" 8^+ state does indeed exist in ^{24}Mg, close to the predicted energy of 11.86 MeV. We shall elaborate on this point further below.

The electric quadrupole matrix elements calculated from the shell-model wave functions of these ^{24}Mg states are presented in Table IV, together with the values of $Q_0(K)$ extracted from them under the assumption that they are members of $K=0$ and $K=2$ bands as noted. The values of $Q(J)$ for the states assigned to the $K=0$ band all have negative signs. This corresponds to a positive value of $Q_0(K=0)$ for each state, consistent with a stable prolate deformation of the underlying intrinsic state of the band. The magnitude of $Q_0(K=0)$ obtained as the average of the values from the 2^+ and 4^+ static moments and the $2^+\leftrightarrow 0^+$ and $4^+\leftrightarrow 2^+$ transition matrix elements is $+57.0\pm1.6$ efm^2, corresponding to $\delta=+0.43$. That this value of δ is 16% smaller than that of ^{20}Ne, while the ^{24}Mg value of $Q_0(K=0)$ is slightly larger than that of ^{20}Ne, reflects the fact that the value of $Q_0(K=0)$ has a dependence on r_{rms} which is divided out of the expression for δ [Eq. (7b)]. The magnitudes of $Q_0(K=0)$ extracted from the static moments of the $K=0$ states with values of J greater than four are smaller than the "band-head" value by factors of 0.8 to 0.5. The $Q_0(K=0)$ magnitudes extracted from the transition matrix elements tend to be still smaller, with the greatest discrepancy from consistency with the features of a $K=0$ rotational band occuring for the 12_2^+ to 10_2^+ transition.

The existence of a $K=2$ band built upon the second $J=2$ state is a common feature of deformed doubly-even nuclei. The energies of ^{24}Mg states obtained from the shell-model calculation exhibit features of such structure, as is evident from Fig. 6(b) and from the electric quadrupole matrix elements of these states presented in Table IV. For a $K=2$ band, the sign of $Q_0(K=2)$ is the same as that of $Q(J)$ for the $J=2$ state and is opposite to that of $Q(J)$ for the states with $J\geq 4$. For $J=3$ the value of $Q(J)$ derived from any finite value of $Q_0(K=2)$ is zero. We see that the calculated value of $Q(J)$ obtained from the shell-model wave function of the first $J=3$ state is indeed very small. Excluding the case of the $J=3$ state, the values extracted for $Q_0(K=2)$ from the values of

$Q(J)$ for the states assumed to belong to $K=2$ band are all positive, corresponding to a stable prolate deformation, similar to what was observed for the $K=0$ band.

For $K\neq 0$ bands we have transitions from states of spin J to states with spins of both $J-1$ and $J-2$. The value of $Q_0(K=2)$ at the band head, obtained as the average of the values extracted from the values of $Q(J)$ for the 2_2^+ and 4_2^+ states and from the transition matrix elements between the states 2_2^+, 3^+, and 4_2^+, is $+58.0\pm2.7$ efm^2 ($\delta=+0.43$). We note that the slightly larger magnitude of $Q_0(K=2)$ relative to $Q_0(K=0)$, which implies a more deformed intrinsic shape, is consistent with the smaller slope (and hence larger moment of inertia) of the $K=2$ $J(J+1)$ line [Fig. 6(b)]. From Table IV we see that the $Q_0(K=2)$ values extracted from the static moments remain near to the band-head value for states of increasing J up through the state of $J=7$, then decrease to about half of this size for the terminal state of the band, and the largest spin for ^{24}Mg, $J=12$. At the higher values of J, the scatter in the values of $Q_0(K=2)$ extracted from the $J\rightarrow J-1$ and $J\rightarrow J-2$ branches of a given state J becomes larger than the deviation of the average value of the $Q_0(K=2)$ of this state from the band-head value.

TABLE IV. Values of calculated electric quadrupole matrix elements $M(E2;J_1\leftrightarrow J_f)$ and $Q(J_i)$ for $T=0$ states in ^{24}Mg together with values of Q_0 extracted from these matrix elements and from corresponding experimental data under the assumption that the states, variously, are members of $K=0$ and $K=2$ rotational bands. The value quoted in the Q, $|M(E2)|$ column are $M(E2)$ when different states J_i and J_f are involved and are Q when the initial and final states J_i are identical. States whose J values are not subscripted are the first occurring states of the respective J-T values. The units are efm^2.

States	Q, $\lvert M(E2)\rvert$	Q_0	Q_0(exp)[a]
	^{24}Mg ($K=0$)		
$2^+\leftrightarrow 0^+$	18.6	59.1	65.8±0.7
$Q(2^+)$	−16.3	+57.2	+63.2±7.0
$4^+\leftrightarrow 2^+$	28.8	57.0	73.1±5.4
$Q(4^+)$	−19.9	+54.6	
$6^+\leftrightarrow 4^+$	33.7	52.9	65.6±16.4
$Q(6^+)$	−16.7	+41.8	
$8_2^+\leftrightarrow 6^+$	28.2	37.8	
$Q(8^+)$	+15.2	−36.1	
$Q(8_2^+)$	−13.7	+32.5	
$10_2^+\leftrightarrow 8_2^+$	11.9	14.2	
$Q(10_2^+)$	−9.59	+22.2	
$12_2^+\leftrightarrow 10_2^+$	0.74	0.80	
$Q(12_2^+)$	−21.1	+47.6	
	^{24}Mg ($K=2$ band)		
$Q(2_2^+)$	+16.6	+58.0	
$3^+\leftrightarrow 2_2^+$	29.3	58.7	<65.6
$Q(3^+)$	−0.055		
$4_2^+\leftrightarrow 2_2^+$	17.8	54.6	82.8±5.9
$4_2^+\leftrightarrow 3^+$	27.5	56.2	
$Q(4_2^+)$	−9.09	+62.5	
$5^+\leftrightarrow 3^+$	23.8	52.0	82.9±5.4
$5^+\leftrightarrow 4_2^+$	26.5	57.9	<69.2
$Q(5^+)$	−13.6	+59.1	
$6_2^+\leftrightarrow 4_2^+$	24.5	44.4	44.9±13.6
$6_2^+\leftrightarrow 5^+$	19.4	45.6	
$Q(6_2^+)$	−20.5	+71.7	
$7^+\leftrightarrow 5^+$	27.5	43.8	
$7^+\leftrightarrow 6_2^+$	24.0	60.1	
$Q(7^+)$	−17.5	+54.1	
$8_3^+\leftrightarrow 6_2^+$	22.1	31.9	
$8_3^+\leftrightarrow 7^+$	20.7	54.9	
$Q(8_3^+)$	−19.9	+56.6	
$9^+\leftrightarrow 7^+$	19.7	26.2	
$9^+\leftrightarrow 8_3^+$	16.7	46.8	
$Q(9^+)$	−8.59	+23.1	
$10^+\leftrightarrow 8_3^+$	14.7	18.3	
$10^+\leftrightarrow 9^+$	19.9	58.5	
$Q(10^+)$	−10.3	+26.6	
$11^+\leftrightarrow 9^+$	8.31	9.76	
$11^+\leftrightarrow 10^+$	16.9	52.0	
$Q(11^+)$	−9.59	+24.0	
$12^+\leftrightarrow 10^+$	16.5	18.3	
$12^+\leftrightarrow 11^+$	22.2	71.2	
$Q(12^+)$	−11.8	+28.7	

[a]Taken from Ref. 7.

As noted, the $K=0$ ground-state band and the $K=2$ excited-state band intersect each other between $J=8$ and $J=10$. The evidence for this appears visually in the $J(J+1)$ excitation energy plot of Fig. 6(b), and from inspection of the values of the $E2$ matrix elements listed in Table IV. Also, as noted, the energy level plots show that the 8_1^+ levels belongs to neither band. This is especially brought out from the $E2$ matrix elements, in that the calculated quadrupole moment calculation for the yrast 8^+ state is $+15.15$ efm^2, opposite in sign to those of the 8^+ states assigned to the $K=0$ ground-state band and to the $K=2$ excited-state band.

The orbit occupancies (Fig. 3) for the presumed $K=0$ states of $J=0$ through $J=6$ in ^{24}Mg are clustered together very tightly. The presumed $J=8$ state of the $K=0$ band has 0.3 units *less* $0d_{5/2}$ occupancy than the average of the lower spin states, perhaps in correlation with the 1.0 unit greater $0d_{5/2}$ occupancy of the yrast 8^+ state. The $1s_{1/2}$ occupancies of the 10_2^+ and 12_2^+ states decrease markedly from the values of the $J^\pi=0^+-6^+$ states, as was also the case for the ^{20}Ne 8^+ level. However, in ^{24}Mg the excess occupancy released from the $1s_{1/2}$ orbit goes into the $0d_{3/2}$ orbit, not the $0d_{5/2}$ orbit as in ^{20}Ne. The occupancies of the states of the $K=2$ band with $J=2-8$ are also tightly clustered, with the excursions associated with higher spins again tending towards exchange of $1s_{1/2}$ for $0d_{3/2}$ particles. The lower-spin states of the two bands are separated from each other (Fig. 3), but beyond $J=8$ the crossing of the bands can be seen also in the mingling of the occupancy paths. The singularity of the lowest-energy 8^+ state is evident in Fig. 3.

As with the case of the $K=0$ and $K=3$ bands in ^{22}Na, we have calculated $E2$ matrix elements between states in the nominal $K=2$ band and states in the nominal $K=0$ band in ^{24}Mg, the values being presented in Table III. The cross-band $E2$ transitions between the low-spin states ($J\leq 9$) are on the average, a factor of 2 smaller than the corresponding in-band $E2$ transition. Similar inhibitions are found for the cross-band $E2$ transitions between states of spins 11^+ and 12^+. The cross-band $E2$ transitions between states of spins 10^+ and 11^+, however, are comparable in strength to the in-band $E2$ transitions. Of

course, this is not unexpected, since it is here [Figs. 3 and 6(b)] that the two bands cross, with a consequent mixing of their structure.

VI. RESULTS FOR ODD-MASS NUCLEI

A. $K=\frac{3}{2}$ bands in ^{21}Ne and ^{23}Na

The $T=\frac{1}{2}$ nuclei of the $A=21$ and $A=23$ systems have $J^\pi=\frac{3}{2}^+$ ground states and experimentally observed features of some of their prominant energy levels which are suggestive of the structure of $K=\frac{3}{2}$ rotational bands. The full *sd*-shell space allows construction of states with spins up to $\frac{19}{2}^+$ for five active particles coupled to $T=\frac{1}{2}$ (^{21}Ne). The maximum dimensionality is 223, for the $J^\pi=\frac{5}{2}^+$ states, and the minimum is two, for $J^\pi=\frac{19}{2}^+$. The eigenvalues obtained for states of ^{21}Ne in the shell-model calculation are shown plotted against the $J(J+1)$ spacing in Fig. 7. The equation of the least-squares fit to these points is $E_x(\text{keV})=141\,J(J+1)-529$, with an rms deviation of 236 keV. The energies of the various states are staggered systematically about the straight line, with the $J^\pi=\frac{5}{2}^+$, $\frac{9}{2}^+$, $\frac{13}{2}^+$, and $\frac{17}{2}^+$ states lying below and the $J^\pi=\frac{7}{2}^+$, $\frac{11}{2}^+$, $\frac{15}{2}^+$, and $\frac{19}{2}^+$ states lying above. This effect is particularly pronounced for the highest three spins.

The electric quadrupole matrix elements calculated from these ^{21}Ne shell-model wave functions, and the values of $Q_0(K=\frac{3}{2})$ extracted from them under the assumption that the states are members of a $K=\frac{3}{2}$ rotational band, are presented in Table V. As seen from Eq. (10), in the case of a $K=\frac{3}{2}$ band the sign of $Q(J)$ is opposite to that of $Q_0(K=\frac{3}{2})$ for $J=\frac{3}{2}$ and of the same sign for states of higher spin. The other qualitative feature of $K=\frac{3}{2}$ bands is that the magnitude of $Q(J)$ for the $J=\frac{5}{2}$ state of the band is much smaller (by a factor of 14) than that of $Q_0(K=\frac{3}{2})$. The values calculated for $Q(J)$ for the various states yield positive signs for each associated $Q_0(K=\frac{3}{2})$. Hence, the results are consistent with the assumption that the wave functions can be interpreted as originating from a $K=\frac{3}{2}$ intrinsic state of prolate deformation. The magnitude of $Q(J=\frac{5}{2})$ is indeed very small. The associated magnitude of $Q_0(K=\frac{3}{2})$ is smaller than the values extracted from neighboring matrix elements, but the change in the value of $Q(J=\frac{5}{2})$ which would be necessary to bring the value of $Q_0(\frac{3}{2})$ into consistency with its neighbors is small relative to the typical scatter (1–2 efm^2) in the shell-model values.

The magnitude of $Q_0(K=\frac{3}{2})$ near the band head is $+48.5\pm2.3$ efm^2, obtained as the average of the values extracted from the $J=\frac{3}{2}$ and $\frac{7}{2}$ static moments and the transition matrix elements between the $J=\frac{3}{2}$, $\frac{5}{2}$, and $\frac{7}{2}$ states. This is equivalent to a value of $\delta=+0.46$. The values of $Q_0(K=\frac{3}{2})$ extracted from the static moments of the higher spin states decrease slowly from the band-head value as J increases, the values for $J=\frac{15}{2}$, $\frac{17}{2}$, and $\frac{19}{2}$ being a factor of 0.8 smaller. The magnitudes of $Q_0(K=\frac{3}{2})$ extracted from the transition matrix elements between states of J and $J+1$ are similar to those extracted from the static moments of these same two states, with a slightly increasing scatter as J increases. The magnitudes of $Q_0(K=\frac{3}{2})$ extracted from the transition matrix elements between states of J and $J+2$ are smaller than those from the corresponding static moment values, however.

The occupation numbers (Fig. 8) for these wave functions are clustered relatively tightly up through $J=\frac{15}{2}$. The $0d_{3/2}$ occupation is quite stable for these states, with the variations taking the form of complementary changes in the $0d_{5/2}$ and $1s_{1/2}$ values. As the spin values increase to the limiting values for the model space, at $J=\frac{17}{2}$ and $\frac{19}{2}$, the variations in occupation number increase in magnitude, with a large increase in $0d_{5/2}$ occupancy for $J=\frac{17}{2}$ followed by a very large increase in the $0d_{3/2}$ occupancy for $J=\frac{19}{2}$. Thus, until Pauli effects become dom-

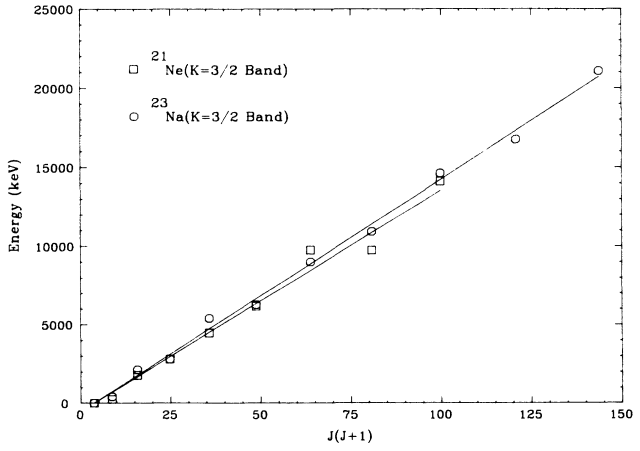

FIG. 7. Plot of E_x vs $J(J+1)$ for the suggested $K=\frac{3}{2}$ bands in ^{21}Ne (squares) and ^{23}Na (circles).

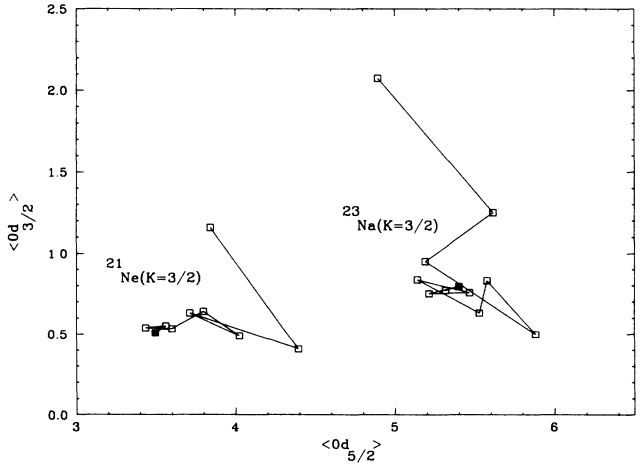

FIG. 8. Occupancy diagram for states in the suggested rotational bands in ^{21}Ne and ^{23}Na. The solid point for each nucleus represents the band head and the points are connected in order of increasing J values.

TABLE V. Values of calculated electric quadrupole matrix elements $M(E2;J_i \leftrightarrow J_f)$ and $Q(J_i)$ for $T=\frac{1}{2}$ states in ^{21}Ne and ^{23}Na, together with values of Q_0 extracted from these matrix elements and from corresponding experimental data under the assumption that the states are members of $K=\frac{3}{2}$ rotational bands. The values quoted in the Q, $|M(E2)|$ column are $M(E2)$ when different states J_i and J_f are involved and are Q when the initial and final states J_i are identical. States whose J values are not subscripted are the first occurring states of the respective J-T values. The units are efm^2.

States	Q, $\lvert M(E2)\rvert$	Q_0	Q_0(exp)[a]
	^{21}Ne ($K=\frac{3}{2}$)		
$Q(\frac{3}{2}^+)$	+10.1	+50.6	+51.6±4.0
$\frac{5}{2}^+ \leftrightarrow \frac{3}{2}^+$	21.4	47.4	49.1±2.7
$Q(\frac{5}{2}^+)$	−1.92	+26.9	
$\frac{7}{2}^+ \leftrightarrow \frac{3}{2}^+$	16.1	47.8	47.3±5.0
$\frac{7}{2}^+ \leftrightarrow \frac{5}{2}^+$	21.3	51.6	40.8±5.9
$Q(\frac{7}{2}^+)$	−9.05	+45.3	
$\frac{9}{2}^+ \leftrightarrow \frac{5}{2}^+$	21.1	45.7	47.8±2.3
$\frac{9}{2}^+ \leftrightarrow \frac{7}{2}^+$	17.9	47.9	45.4±11.4
$Q(\frac{9}{2}^+)$	−12.6	+46.1	
$\frac{11}{2}^+ \leftrightarrow \frac{7}{2}^+$	24.0	43.6	46.0±9.2
$\frac{11}{2}^+ \leftrightarrow \frac{9}{2}^+$	17.4	50.8	40.3±13.0
$Q(\frac{11}{2}^+)$	−14.8	+46.5	
$\frac{13}{2}^+ \leftrightarrow \frac{9}{2}^+$	24.0	38.4	
$\frac{13}{2}^+ \leftrightarrow \frac{11}{2}^+$	12.9	40.6	
$Q(\frac{13}{2}^+)$	−15.4	+44.0	
$\frac{15}{2}^+ \leftrightarrow \frac{11}{2}^+$	22.7	33.0	
$\frac{15}{2}^+ \leftrightarrow \frac{13}{2}^+$	10.7	36.1	
$Q(\frac{15}{2}^+)$	−15.5	+41.6	
$\frac{17}{2}^+ \leftrightarrow \frac{13}{2}^+$	21.3	28.7	
$\frac{17}{2}^+ \leftrightarrow \frac{15}{2}^+$	11.4	40.9	
$Q(\frac{17}{2}^+)$	−15.5	+39.8	
$\frac{19}{2}^+ \leftrightarrow \frac{15}{2}^+$	19.0	23.9	
$\frac{19}{2}^+ \leftrightarrow \frac{17}{2}^+$	7.95	30.1	
$Q(\frac{19}{2}^+)$	−16.3	+40.4	
	^{23}Na ($K=\frac{3}{2}$)		
$Q(\frac{3}{2}^+)$	+10.4	+52.0	+50.3±1.0
$\frac{5}{2}^+ \leftrightarrow \frac{3}{2}^+$	24.1	53.3	55.2±3.3
$Q(\frac{5}{2}^+)$	−2.3	+32.6	
$\frac{7}{2}^+ \leftrightarrow \frac{3}{2}^+$	16.8	49.7	56.0±3.2
$\frac{7}{2}^+ \leftrightarrow \frac{5}{2}^+$	20.9	50.6	49.3±5.1
$Q(\frac{7}{2}^+)$	−10.2	+50.8	
$\frac{9}{2}^+ \leftrightarrow \frac{5}{2}^+$	22.3	48.4	59.4±1.8
$\frac{9}{2}^+ \leftrightarrow \frac{7}{2}^+$	19.8	53.0	108.5±27.2
$Q(\frac{9}{2}^+)$	−11.9	+43.7	
$\frac{11}{2}^+ \leftrightarrow \frac{7}{2}^+$	26.0	47.1	33.7±11.4
$\frac{11}{2}^+ \leftrightarrow \frac{9}{2}^+$	17.5	51.2	39.1±13.1
$Q(\frac{11}{2}^+)$	−14.0	+44.0	
$\frac{13}{2}^+ \leftrightarrow \frac{9}{2}^+$	23.4	39.2	
$\frac{13}{2}^+ \leftrightarrow \frac{11}{2}^+$	11.6	38.3	
$Q(\frac{13}{2}^+)$	−13.2	+37.7	
$\frac{15}{2}^+ \leftrightarrow \frac{11}{2}^+$	26.3	40.2	
$\frac{15}{2}^+ \leftrightarrow \frac{13}{2}^+$	7.06	25.0	
$Q(\frac{15}{2}^+)$	−9.83	+26.4	
$\frac{17}{2}^+ \leftrightarrow \frac{13}{2}^+$	21.2	28.4	
$\frac{17}{2}^+ \leftrightarrow \frac{15}{2}^+$	14.4	51.6	
$Q(\frac{17}{2}^+)$	−12.2	+31.2	
$\frac{19}{2}^+ \leftrightarrow \frac{15}{2}^+$	10.7	13.4	
$\frac{19}{2}^+ \leftrightarrow \frac{17}{2}^+$	16.1	60.8	
$Q(\frac{19}{2}^+)$	−14.1	+34.9	
$\frac{21}{2}^+ \leftrightarrow \frac{17}{2}^+$	8.64	10.2	
$\frac{21}{2}^+ \leftrightarrow \frac{19}{2}^+$	8.58	34.1	
$Q(\frac{21}{2}^+)$	−10.1	+24.5	
$\frac{23}{2}^+ \leftrightarrow \frac{19}{2}^+$	6.92	7.43	
$\frac{23}{2}^+ \leftrightarrow \frac{21}{2}^+$	15.8	65.7	
$Q(\frac{23}{2}^+)$	−15.9	+37.7	

[a]Taken from Ref. 7.

inant near the shell-model termination of the "band," the occupancies of the states are quite constant. Together with the close adherance of the energies to the $J(J+1)$ line and the constancy of $Q_0(K=\frac{3}{2})$, these results suggest a well developed intrinsic deformation underlying this group of states.

The full *sd*-shell space allows construction of states with spins up to $\frac{23}{2}^+$ for seven active particles coupled to $T=\frac{1}{2}$ (^{23}Na). The maximum dimensionality is 1158, for the $J=\frac{7}{2}$ states, and the minimum is three, for $J=\frac{23}{2}$. The eigenvalues obtained for states in ^{23}Na in the shell-model calculation are shown plotted against the $J(J+1)$ spacing in Fig. 7. The equation of the least-squares fit to these points is E_x(keV)$=148\,J(J+1)-550$, with an rms deviation of 133 keV. The energies of the $A=23$ states are staggered systematically about the straight line in the same fashion observed for the $A=21$ example, although the effect is not so pronounced.

The electric quadrupole matrix elements calculated from the shell-model wave functions of these states of ^{23}Na, and the values of $Q_0(K=\frac{3}{2})$ extracted from them under the assumption that the states are members of a $K=\frac{3}{2}$ rotational band, are presented in Table V. The magnitude of $Q_0(K=\frac{3}{2})$ near the band head is $+51.3\pm1.2$ efm^2, obtained as the average of the values extracted from the $J=\frac{3}{2}$ and $\frac{7}{2}$ static moments and the transition matrix elements between the $J=\frac{3}{2}$, $\frac{5}{2}$, and $\frac{7}{2}$ states. This is equivalent to a value of $\delta=+0.43$. As with the $A=21$ system, the magnitude of $Q(J=\frac{5}{2})$ is very small, as is required by Eq. (10). Again, the associated value of $Q_0(K=\frac{3}{2})$ is smaller than the values extracted from neighboring matrix elements, but by an amount that is small relative to the typical scatter in the underlying shell-model values. The relationships between $Q(J)$ and $Q_0(K=\frac{3}{2})$ discussed above for the $A=21$ example hold identically here. Likewise, we observe the same qualitative features in the calculated and extracted values

of $Q(J)$ and $Q_0(K=\frac{3}{2})$.

As with the $A=21$ system, the occupation numbers (Fig. 8) for these $A=23$ wave functions are relatively tightly clustered up through $J=\frac{15}{2}$. As the spin values increase to the limiting values for the model space, at $J=\frac{17}{2}-\frac{23}{2}$, the variations in occupation numbers increase in magnitude, with a large increase in $0d_{5/2}$ occupancy for $J=\frac{17}{2}$ followed by a very large increase in $0d_{3/2}$ occupancy for $J=\frac{19}{2}$, $\frac{21}{2}$, and, especially, $\frac{23}{2}$. The overall results for $A=23$ are thus strikingly similar to those for $A=21$, with the extra model particles apparently contributing to a somewhat more stable intrinsic state and, of course, a higher value of the angular momentum at which the band terminates.

VII. SUMMARY AND CONCLUSIONS

We have examined shell-model calculations of energies and electric quadrupole matrix elements for $A=20-28$ nuclei for characteristic features which would suggest that the levels in question are members of pure rotational bands built upon stable, deformed intrinsic shapes. Unlike experimental data, these model results yield complete sets of precise values for all observables, in particular for quadrupole moments of all states.

The critical features, which are taken as evidence that the levels of a group belong to a given band, are a linear dependence of excitation energies $E_x(J)$ upon the values of $J(J+1)$, a common sign for the intrinsic quadrupole moments extracted from the static quadrupole moments, and approximately equal magnitudes for all the intrinsic quadrupole moment values extracted from transition and moment matrix elements. Such features emerge most clearly in ^{21}Ne and ^{23}Na (apparent $K=\frac{3}{2}$ bands), in ^{20}Ne, ^{22}Ne, and ^{28}Si (apparent $K=0$, J-even bands), in ^{22}Na (apparent $K=0$, J odd, and $K=3$ bands), and in ^{24}Mg (apparent $K=0$, J even, and $K=2$ bands). In contrast, the ^{26}Mg nucleus exhibits no convincing evidence for simple band structure beyond a few enhanced values of electric quadrupole matrix elements. These features of ^{26}Mg are similar to those we calculate for the neighboring nuclei ^{27}Al and ^{25}Mg. While there is some significant evidence for $K=\frac{1}{2}$ and $K=\frac{5}{2}$ band structure in the ^{25}Mg wave functions, the bands cannot be extrapolated neatly to higher J values. In ^{27}Al, the electromagnetic matrix elements allow very little inference of simple band structure at all.

A general and, of course, inevitable feature of shell-model results in any specific model space is that there is a maximum possible value of the total angular momentum J for each nucleus, the so-called "band cutoff" value of J. For the *sd*-shell examples studied, the cutoff values of J range from $J=8$ to 14. The experimental existence of band cutoffs has been an interesting but unresolved issue for some time. In the context of the present study, the issue is the degree to which the band properties which characterize the levels near the lowest value of J, the "band head," persist unmodified up to the cutoff value.

In the nuclei with the most clearly developed band structures, the values of the intrinsic quadrupole moments extracted from the matrix elements involving the lowest several J values typically vary by only 2–3 % from each other, with the values from the quadrupole moment of the lowest state and from the transitions to the lowest state being very close to each other. The exceptions to this stability of extracted values of $Q_0(K)$ at low values of J occur in the $K\neq 0$ bands, at those J values for which the ratio of $Q_0(K)$ to $Q(JK)$ is very large. These cases necessarily involve very small values of the shell-model predictions relative to the single-particle values. As the values of J increase up to the cutoff J values of the "bands," the values of $Q_0(K)$ extracted from the static quadrupole moments retain the same sign and approximate magnitude, while the magnitudes of $Q_0(K)$ extracted from the transition matrix elements show increasing fluctuations towards smaller values, with the typical excursions from the "band-head" values of $Q_0(K)$ being 20–50 %.

The existence of a well-defined band does not seem correlated with extraordinarily large values of deformation. All of the systems considered have comparable magnitudes of δ as inferred from the levels near the band head. These inferred deformations are largely independent of the number of active particles in the model space, the ^{20}Ne system, with only four particles, having a slightly larger value than any of the "heavier" (five to twelve particle) systems. The quantitative degree of stability in the band parameters does seem positively correlated with shell-model dimensions, however, with the smaller systems such as ^{20}Ne showing symptoms of not having enough wave function components to generate the coherent interference necessary for smooth propagation of the $E2$ band features from level to level.

The energies of the levels in these bands follow similar trends, with close adherance of the $J(J+1)$ line at low values of J giving way to larger, typically oscillating, excursions as the cutoff value is approached. In the $K=0$ bands, the energies of the 2^+ and 4^+ levels always fall above the straight lines which give the best fit to the entire set of energies. The two $K=\frac{3}{2}$ bands show a systematic staggering about the best-fit lines, with the second, $\frac{5}{2}^+$, states already showing the effect clearly. The fluctuations in energy values near cutoff values of J tend to be correlated with the shell-model dimensions, the largest energy deviations occuring for the cases in which the dimensions are smallest.

The correlation of well-defined band properties with tightly grouped points in the plots of the occupancy diagram of the shell-model orbits is positive overall, but with some significant exceptions. As with values of energies and $Q_0(K)$, the occupation numbers of the shell-model orbitals are more stable for wave functions near the band head than near the band cutoff. The excursions of the occupancies from the "average" values for the bands near and at the cutoff values of J are more striking than are those for the values of energies and $Q_0(K)$. Of course, the occupancies in a sense are a direct reflection of the cutoff phenomena, so this is not surprising. In the instances for which two bands are identified in a single nucleus, the occupancy points for the lower J members fall into distinctly different areas of the diagram.

These features would seem to confirm the conjecture of Watt *et al.*, that the orbit occupation numbers are keys to identifying and characterizing a band within the shell-model representation. However, ^{28}Si provides an instructive counterexample. The bands found in the $A=21-24$ systems occur in the "middle" of the $0d_{5/2}$ subshell. Up until the band-cuttoff values, different values of J can be formed without the necessity of transfering particles from one orbit to another. It could be presumed that this "distance" from the effects of shell closure is a prerequisite for the emergence of well-developed bands. The example of ^{28}Si contradicts this presumption. In the context of $Q_0(K)$ values and, up to $J=8$, energies, there is striking evidence of a $K=0$ band in ^{28}Si. This "band" thus occurs directly upon a minor shell closure (filling of the $0d_{5/2}$ subshell). The points in the occupancy diagram for ^{28}Si show the excursion necessary to build states of successive higher J values upon the foundation of a shell closure. Nonetheless, these excursions in occupancy apparently fail to affect the energies and electric quadrupole matrix elements of the states.

In summary, shell-model wave functions for several nuclei in the $A=20-28$ region exhibit very stable rotational-band characteristics for the lowest several values of J in the band sequence. In these systems the features of band structure has been traced, with diminishing quantitative accuracy, all the way to the highest allowed values of J in the shell-model space. Results for other systems in this region show little evidence for band structure beyond a few enhanced $E2$ matrix elements and the inevitable increase of excitation energy with increasing angular momentum. Clustering of orbit occupation numbers is a frequent, but not inevitable, corollary of a well-developed band structure.

This work was supported in part by National Science Foundation Grant No. 85-09736.

[1]A. Bohr and B. R. Mottelson, Mat. Fys. Med. Dan. Vid. Selsk. **27**, No. 16 (1953).
[2]A. E. Litherland *et al.*, Can. J. Phys. **36**, 378 (1958) and references therein.
[3]Kumar H. Bhatt, Nucl. Phys. **39**, 375 (1962).
[4]D. A. Bromley, H. E. Grove, and A. E. Litherland, Can. J. Phys. **35**, 1057 (1957).
[5]A. J. Howard, J. P. Allen, and D. A. Bromley, Phys. Rev. **139**, B1135 (1965).
[6]B. H. Wildenthal, Prog. Part. Nucl. Phys. **11**, 5 (1983).
[7]B. H. Wildenthal, J. Keinonen, and B. A. Brown (unpublished).
[8]B. A. Brown *et al.*, Phys. Rev. C **26**, 2247 (1982); B. A. Brown, W. Chung, and B. H. Wildenthal, *ibid.* **22**, 774 (1980).
[9]P. J. Brussaard and P. W. M. Glaudemans, *Shell-Model Applications in Nuclear Spectroscopy* (North-Holland, Amsterdam, 1977).
[10]Amos deShalit and Herman Feshbach, *Theoretical Nuclear Physics Volume 1: Nuclear Structure* (Wiley, New York, 1974).
[11]M. A. Preston and R. K. Bhaduri, *Structure of the Nucleus* (Addison Wesley, Reading Masschusetts, 1975).
[12]A. Watt, D. Kelvin, and R. R. Whitehead, Phys. Lett. **63B**, 388 (1976).
[13]A. Watt, D. Kelvin, and R. R. Whitehead, J. Phys. G **6**, 35 (1980).
[14]R. D. Lawson, *Theory of the Nuclear Shell Model* (Clarendon, Oxford, 1980).
[15]F. Glatz *et al.*, Z. Phys. A **324**, 187 (1986).
[16]B. M. Preedom and B. H. Wildenthal, Phys. Rev. C **6**, 1633 (1972).
[17]W. Chung, Ph.D. thesis, Michigan State University, 1976 (unpublished).
[18]T. T. S. Kuo and G. E. Brown, Nucl. Phys. **85**, 40 (1966).
[19]D. Branford, M. J. Spooner, and I. F. Wright, Part. Nucl. **4**, 231 (1972).